

High-Speed Finite Control Set Model Predictive Control for Power Electronics

Bartolomeo Stellato and Paul J. Goulart

Abstract

Common approaches for direct model predictive control (MPC) for current reference tracking in power electronics suffer from the high computational complexity encountered when solving integer optimal control problems over long prediction horizons. We propose an efficient alternative method based on approximate dynamic programming, greatly reducing the computational burden and enabling sampling times under $25 \mu\text{s}$. Our approach is based on the offline minimization of an infinite horizon cost function estimate which is then applied to the tail cost of the MPC problem. This allows us to reduce the controller horizon to a very small number of stages improving overall controller performance. Our proposed algorithm is validated on a variable speed drive system with a three-level voltage source converter.

Index Terms

Approximate dynamic programming, drive systems, finite control set, integer programming, model predictive control (MPC).

I. INTRODUCTION

AMONG the control strategies adopted in power electronics, model predictive control (MPC) [1] has recently gained popularity due to its various advantages [2]. MPC has been shown to outperform traditional control methods mainly because of its ease in handling time-domain constraint specifications that can be imposed by formulating the control problem as a constrained optimization problem. Due to its structure, MPC can be used for several power systems topologies and operating conditions providing a greater degree of flexibility compared to traditional approaches.

In power electronics, many conventional control strategies are based on proportional-plus-integral (PI) controllers providing continuous input signals to a modulator, which manages conversion to discrete switching positions. Direct MPC [3], instead combines the current control and the modulation problem into a single computational problem, providing a powerful alternative to conventional PI controllers. With direct MPC, the manipulated variables are the switch positions, which lie in a discrete and finite set, giving rise to a switched system.

The authors are with the University of Oxford, Parks Road, Oxford, OX1 3PJ, U.K. (e-mail: bartolomeo.stellato@eng.ox.ac.uk; paul.goulart@eng.ox.ac.uk).

This work was supported by the People Programme (Marie Curie Actions) of the European Unions Seventh Framework Programme (FP7/2007-2013) under REA grant agreement no 607957 (TEMPO).

Therefore, this approach does not require a modulator and is often referred to as *finite control set* MPC.

Since the manipulated variables are restricted to be integers, the optimization problem underlying direct MPC is provably \mathcal{NP} -hard [4]. In power electronics, these optimization problems are often solved by complete enumeration of all the possible solutions which grow exponentially with the prediction horizon [5]. Since long horizons are required to ensure stability and good closed-loop performance [6], direct MPC quickly becomes intractable for real-time applications. As a consequence, in cases when reference tracking of the converter currents is considered, the controller horizon is often restricted to one [2]. Despite attempts to overcome the computational burden of these methods [7], the problem remains open to allow implementation of these algorithms on embedded systems.

A recent technique introduced in [8] and benchmarked in [9], reduces the computational burden of direct MPC when increasing the prediction horizon. In that work the optimization problem was formulated as an integer least-squares (ILS) problem and solved using a tailored branch-and-bound algorithm, described as *sphere decoding* [10], generating the optimal switching sequence at each time step. Although this approach appears promising relating to previous work, the computation time required to perform the sphere decoding algorithm for long horizons (i.e. $N = 10$), is still far slower than the sampling time typically required, i.e. $T_s = 25 \mu\text{s}$.

This paper introduces a different method to deal with the direct MPC problem. In contrast to common formulations [11] where the switching frequency is controlled indirectly via penalization of the input switches over the controller horizon, in this work the system dynamics are augmented to directly estimate the switching frequency. Our formulation allows the designer to set the desired switching frequency a priori by penalizing its deviations from this estimate. Thus, the cost function tuning can be performed more easily than with the approach in [9] and [8] where a tuning parameter spans the whole frequency range with no intuitive connection to the desired frequency. To address the computational issues of long prediction horizons, we formulate the tracking problem as a regulation one by augmenting the state dynamics and cast it in the framework of approximate dynamic programming (ADP) [12]. The infinite horizon tail cost is approximated using the approach in [13] and [14] by solving a semidefinite program (SDP) [15] offline. This enables us to shorten the controller horizon by applying the estimated tail cost to the last stage and to keep good control performance.

Simulation results show that with our method, even very short prediction horizons gives better performances than the approach in [9] and [8] with much longer planning horizons, while drastically reducing the computational burden. Moreover, with a simple complexity analysis we show that our approach could be implemented in a parallelised fashion on embedded platforms and run comfortably within a $25 \mu\text{s}$ sampling time.

As a case study, our proposed approach is applied to a variable-speed drive system consisting of a three-level neutral point clamped voltage source inverter connected to a medium-voltage induction machine. The plant is modelled as a linear system with a switched three-phase input with equal switching steps for all phases.

The remainder of the paper is organized as follows. In Section II we describe the drive system case study and derive the physical model. In Section III the direct MPC problem is derived by augmenting the state dynamics and approximating the infinite horizon tail cost using ADP. We study the computational complexity of the proposed approach in Section IV. Finally, we show the simulation results on the derived model in Section VI and provide conclusions in Section VII.

In this work we use normalized quantities by adopting the per unit system (pu). The time scale t is also normalized using the base angular velocity ω_b that in this case is $2\pi \cdot 50$ rad/s, i.e. one time unit in the per unit system corresponds to $1/\omega_b$ s. Variables in the three-phase system (abc) are denoted $\xi_{abc} = [\xi_a \ \xi_b \ \xi_c]^\top$. It is common practice to transform phase variables to $\xi_{\alpha\beta}$ in the stationary orthogonal $\alpha\beta$ coordinates by $\xi_{\alpha\beta} = \mathbf{P}\xi_{abc}$. The inverse operation can be performed as $\xi_{abc} = \mathbf{P}^\dagger\xi_{\alpha\beta}$. The matrices \mathbf{P} and \mathbf{P}^\dagger are the Park transform and its pseudoinverse respectively, i.e.

$$\mathbf{P} = \frac{2}{3} \begin{bmatrix} 1 & -\frac{1}{2} & -\frac{1}{2} \\ 0 & \frac{\sqrt{3}}{2} & -\frac{\sqrt{3}}{2} \end{bmatrix}, \quad \mathbf{P}^\dagger = \begin{bmatrix} 1 & 0 \\ -\frac{1}{2} & \frac{\sqrt{3}}{2} \\ \frac{1}{2} & -\frac{\sqrt{3}}{2} \end{bmatrix}.$$

II. DRIVE SYSTEM CASE STUDY

In this work we consider a variable speed drive system consisting of a three-level neutral point clamped (NPC) voltage source inverter driving a medium-voltage (MV) induction machine shown in Figure 1. The total dc-link voltage V_{dc} is assumed to be constant and the neutral point potential N fixed.

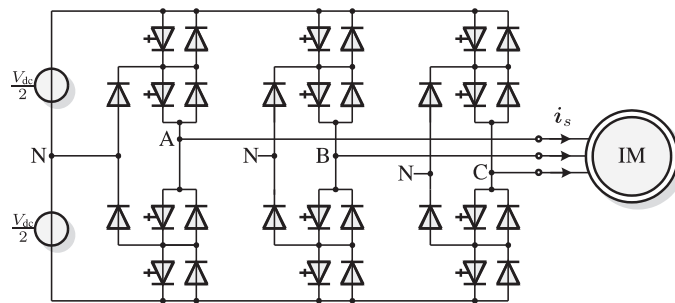


Fig. 1. Three-level three-phase neutral point clamped (NPC) voltage source inverter driving an induction motor with a fixed neutral point potential. Image taken from [8].

A. Physical Model of the Inverter

The switch positions in the three-phase legs can be described by the integer input variables $u_a, u_b, u_c \in \{-1, 0, 1\}$, leading to phase voltages $\{-\frac{V_{dc}}{2}, 0, \frac{V_{dc}}{2}\}$, respectively. Hence, the output voltage of the inverter is given by

$$\mathbf{v}_{\alpha\beta} = \frac{V_{dc}}{2} \mathbf{u}_{\alpha\beta} = \frac{V_{dc}}{2} \mathbf{P} \mathbf{u}_{sw}, \quad (1)$$

where

$$\mathbf{u}_{sw} = [u_a \quad u_b \quad u_c]^T.$$

The possible voltage switches are displayed in Figure 2.

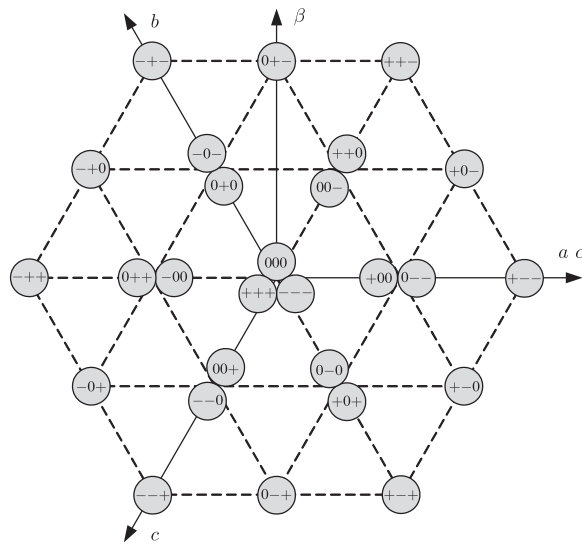


Fig. 2. Voltage vectors generated by a three-level inverter shown in the $\alpha\beta$ plane together with the three-phase positions of \mathbf{u}_{sw} (+ corresponds to 1 and - to -1). Image taken from [8].

B. Physical Model of the Machine

Hereafter we derive the state-space model of the squirrel-cage induction machine in the $\alpha\beta$ plane. Since we are considering a current control problem, it is convenient to use the stator current $\mathbf{i}_{s,\alpha\beta}$ and the rotor flux $\psi_{r,\alpha\beta}$ as state variables. The model input is the stator voltage $\mathbf{v}_{s,\alpha\beta}$ which is equal to the inverter output voltage in (1). The model parameters are stator and rotor resistances R_s and R_r , the mutual, stator and rotor reactances X_m, X_{ls} and X_{lr}

respectively, the inertia J and the mechanical load torque T_l . Given these quantities, the continuous-time state equations [16], [17] are

$$\begin{aligned}\frac{d\mathbf{i}_s}{dt} &= -\frac{1}{\tau_s}\mathbf{i}_s + \left(\frac{1}{\tau_r}\mathbf{I} - \omega_r \begin{bmatrix} 0 & -1 \\ 1 & 0 \end{bmatrix}\right) \frac{X_m}{D}\boldsymbol{\psi}_r + \frac{X_r}{D}\mathbf{v}_s \\ \frac{d\boldsymbol{\psi}_r}{dt} &= \frac{X_m}{\tau_r}\mathbf{i}_s - \frac{1}{\tau_r}\boldsymbol{\psi}_r + \omega_r \begin{bmatrix} 0 & -1 \\ 1 & 0 \end{bmatrix}\boldsymbol{\psi}_r \\ \frac{d\omega_r}{dt} &= \frac{1}{J}(T_e - T_l),\end{aligned}\quad (2)$$

where $D := X_s X_r - X_m^2$ with $X_s := X_{ls} + X_m$ and $X_r := X_{lr} + X_m$, and \mathbf{I} represents the 2×2 identity matrix. To simplify the notation, we have dropped the subscripts $\alpha\beta$ from all vectors in (2). Moreover, $\tau_s := X_r D / (R_s X_r^2 + R_r X_m^2)$ and $\tau_r := X_r / R_r$ are the stator and the rotor time constants respectively. The electromagnetic torque is given by $T_e := X_m / X_r (\boldsymbol{\psi}_s \times \mathbf{i}_s)$. The rotor speed ω_r is assumed to be constant within the prediction horizon. For prediction horizons on the order of a few milliseconds this is a mild assumption.

C. Complete Model of the Physical System

Given models of the drive and of the induction motor in (1) and (2) respectively, the state-space model in the continuous time domain can be described as

$$\frac{d\mathbf{x}_{ph}(t)}{dt} = \mathbf{D}\mathbf{x}_{ph}(t) + \mathbf{E}\mathbf{u}_{sw}(t) \quad (3a)$$

$$\mathbf{y}_{ph}(t) = \mathbf{F}\mathbf{x}_{ph}(t), \quad (3b)$$

where the state vector $\mathbf{x}_{ph} = [i_{s,\alpha} \ i_{s,\beta} \ \psi_{r,\alpha} \ \psi_{r,\beta}]$, includes the stator current and rotor flux in the $\alpha\beta$ reference frame. The output vector is taken as the stator current, i.e. $\mathbf{y}_{ph} = \mathbf{i}_s$. The matrices \mathbf{D} , \mathbf{E} and \mathbf{F} can be found in Appendix A.

The state-space model of the drive can be converted in discrete-time using exact Euler discretization. By integrating (3a) from $t = k\hat{T}_s$ to $t = (k+1)\hat{T}_s$ and keeping $\mathbf{u}_{sw}(t)$ constant during each interval and equal to $\mathbf{u}_{sw}(k)$, the discrete-time model becomes

$$\mathbf{x}_{ph}(k+1) = \mathbf{A}_{ph}\mathbf{x}_{ph}(k) + \mathbf{B}_{ph}\mathbf{u}_{sw}(k) \quad (4a)$$

$$\mathbf{y}_{ph}(k) = \mathbf{C}_{ph}\mathbf{x}_{ph}(k), \quad (4b)$$

with $k \in \mathbb{N}$ and matrices $\mathbf{A}_{ph} := e^{D\hat{T}_s}$, $\mathbf{B}_{ph} := -D^{-1}(\mathbf{I} - \mathbf{A}_{ph})\mathbf{E}$ and $\mathbf{C}_{ph} := \mathbf{F}$. \mathbf{I} is an identity matrix of appropriate dimensions. Although the sampling time is $T_s = 25 \mu\text{s}$, we use the discretization interval $\hat{T}_s = T_s \omega_b$ for consistency with our per unit system, where ω_b is the base frequency.

III. MODEL PREDICTIVE CURRENT CONTROL

A. Problem Description

Our control scheme must address address two conflicting objectives simultaneously. On one hand, the distortion of the stator currents \mathbf{i}_s corresponds to ripples in the torque of the motor

that are the main source of mechanical stress on the load and the bearings. In order to reduce damage to the machine and the load, the distortion of stator currents must be kept as low as possible. On the other hand, high frequency switching of the inputs \mathbf{u}_{sw} produces high power losses and stress on the physical devices. To reduce the energy needed and to preserve the lifespan of the components, we therefore should minimize the switching frequency of the integer inputs. In power converters, there is an unavoidable tradeoff between these two criteria.

In contrast to the common approaches in direct MPC where the switching frequency is minimized, in this work we will penalize its difference from the desired frequency, denoted f_{sw}^* . This is motivated by the fact that drives are usually designed to run at a specific nominal switching frequency and the control algorithms are typically tuned to match this requirement.

The current distortion is measured via the total harmonic distortion (THD). Given an infinitely long time-domain current signal i and its fundamental component i^* of magnitude 1, we define the THD as the ratio between the root mean square (RMS) of their difference and the RMS of i^* . Since i^* is sinusoidal, its RMS value is $1/\sqrt{2}$. Hence, we can write the the THD as

$$THD := \sqrt{2}\text{RMS}(i - i^*). \quad (5)$$

It is of course not possible to calculate the THD in real time within our controller computations because of finite storage constraints.

The switching frequency of the inverter can be identified by computing the average frequency of each active semiconductor device. As displayed in Figure 1, the total number of switches for all three phases is 12, and for every transition of each phase u_a, u_b, u_c between different adjacent switch positions one physical device is turned on. Given $2M \in \mathbb{N}$ time steps, it is possible to estimate the switching frequency of every device by counting the number of *on* transitions over the time interval and dividing the sum by the interval's length. Then, we can average over all the physical switches by dividing the computed fraction by 12. At time k , the switching frequency estimate can be written as

$$f_{sw,M}(k) := \frac{1}{12 \cdot 2M \cdot T_s} \sum_{i=-M}^M \|\mathbf{u}_{sw}(k+i) - \mathbf{u}_{sw}(k+i-1)\|_1, \quad (6)$$

that corresponds to a non-causal finite impulse response (FIR) filter of order $2M$. The true average switching frequency is the limit of this quantity as the window length goes to infinity

$$f_{sw} := \lim_{M \rightarrow \infty} f_{sw,M}(k), \quad (7)$$

and does not depend on time k .

The f_{sw} computation brings similar issues as the THD. In addition to finite storage constraints, the part of the sum regarding the future signals produces a non-causal filter that is impossible to implement in a real time control scheme.

These issues in computing THD and f_{sw} will be addressed in the following two sections via augmentation of our state space model to include suitable approximation schemes for both quantities.

B. Total Harmonic Distortion

By definition, the THD can be minimized by reducing the effect of the ripples in the produced currents.

The three reference phase sinusoids \mathbf{i}_s^* are defined in the normalized per unit (pu) time scale and have shifted phases (in seconds, these signals oscillate at frequency ω_b)

$$\mathbf{i}_s^*(k) = \left[\sin(k) \quad \sin\left(k - \frac{2}{3}\pi\right) \quad \sin\left(k - \frac{4}{3}\pi\right) \right]^\top.$$

It is straightforward to show (see [18]) that the corresponding reference currents in the $\alpha\beta$ reference frame are

$$\mathbf{i}_{s,\alpha\beta}^*(k) = \left[\sin(k) \quad -\cos(k) \right]^\top. \quad (8)$$

From the stator currents in $\alpha\beta$ frame, the ripples can be obtained by subtracting the perfect sinusoids that need to be tracked, producing the error signal $\mathbf{e}_i(k) := \mathbf{i}_{s,\alpha\beta}(k) - \mathbf{i}_{s,\alpha\beta}^*(k)$. In order to minimize a reasonable approximation of the THD defined in (5) for both dimensions $\alpha\beta$, in our controller we minimize the squared 2-norm of \mathbf{e}_i for all future time instants. We also introduce a discount factor $\gamma \in (0, 1)$ to normalize the summation preventing it from going to infinity in case of persistent error. The cost function related to THD minimization is, therefore,

$$\sum_{k=0}^{\infty} \gamma^k \|\mathbf{e}_i(k)\|_2^2. \quad (9)$$

In order to construct a regulation problem, we will include the oscillating currents from (8) as two additional uncontrollable states $\mathbf{x}_{osc} = \mathbf{i}_{s,\alpha\beta}^*$ within our model of the system dynamics. The ripple signal $\mathbf{e}_i(k)$ is then modeled as an output defined by the difference between two pairs of system states.

C. Switching Frequency

To overcome the difficulty of dealing with the filter in (6), we will consider only the past input sequence, with negative time shift giving a causal FIR filter estimating f_{sw} . This filter will be approximated with an infinite impulse response (IIR) one whose dynamics can be modeled as a linear time invariant (LTI) system. Note that future input sequences in (6) will be taken into account inside the controller prediction.

Let us define three binary phase inputs denoting whether each phase switching position changed at time k or not,

$$\mathbf{p}(k) = \left[p_a(k) \quad p_b(k) \quad p_c(k) \right]^\top \in \{0, 1\}^3, \quad (10)$$

with

$$p_s(k) = \|u_s(k) - u_s(k-1)\|_1, \quad s \in \{a, b, c\}. \quad (11)$$

It is straightforward to show that the following second order IIR filter will approximate the one-sided version of the FIR filter in (6) [19]:

$$\begin{aligned}\mathbf{x}_{flt}(k+1) &= \begin{bmatrix} a_1 & 0 \\ 1-a_1 & a_2 \end{bmatrix} \mathbf{x}_{flt}(k) + \frac{1-a_2}{12T_s} \begin{bmatrix} 1 & 1 & 1 \\ 0 & 0 & 0 \end{bmatrix} \mathbf{p}(k) \\ \hat{f}_{sw}(k) &= [0 \quad 1] \mathbf{x}_{flt}(k),\end{aligned}$$

where $\hat{f}_{sw}(k)$ is the estimated switching frequency. The two poles in $a_1 = 1 - 1/r_1$ and $a_2 = 1 - 1/r_2$ with $r_1, r_2 \gg 0$ can be tuned to shape the behavior of the filter. By increasing a_1, a_2 , the estimate becomes smoother while decreasing a_1, a_2 gives a faster estimation with more noisy values. We will denote the difference between the approximation $\hat{f}_{sw}(k)$ and the target frequency f_{sw}^* by $e_{sw}(k) := \hat{f}_{sw}(k) - f_{sw}^*(k)$.

Therefore, the quantity to be minimized in order to bring the switching frequency estimate as close to the target as possible is

$$\sum_{k=0}^{\infty} \delta \cdot \gamma^k \|e_{sw}(k)\|_2^2, \quad (12)$$

where $\delta \in \mathbb{R}_+$ is a design parameter included to reflect the relative importance of this part of the cost relative to the THD component.

Finally, we can augment the state space to include the filter dynamics and the target frequency by adding the states $[\mathbf{x}_{flt}^\top \quad f_{sw}^*]^\top$ so that the control inputs try to drive the difference between two states to zero. Since the physical states are expressed in per unit (pu) system with values around 1, in order to have these augmented states within the same order of magnitude, we will normalize them by the desired frequency f_{sw}^* defining $\mathbf{x}_{sw} = [(1/f_{sw}^*)\mathbf{x}_{flt}^\top \quad 1]^\top$.

D. MPC Problem Formulation

Let us define the complete augmented state as

$$\mathbf{x}(k) := [\mathbf{x}_{ph}(k)^\top \quad \mathbf{x}_{osc}(k)^\top \quad \mathbf{x}_{sw}(k)^\top \quad \mathbf{u}_{sw}(k-1)^\top]^\top, \quad (13)$$

with $\mathbf{x}(k) \in \mathbb{R}^9 \times \{-1, 0, 1\}^3$ and total state dimension $n_x = 12$. Vector \mathbf{x}_{ph} represents the physical system from Section II-C, \mathbf{x}_{osc} defines the oscillating states of the sinusoids to track introduced in Section III-B, $\mathbf{u}_{sw}(k-1)$ are additional states used to keep track of the physical switching positions at the previous stage and \mathbf{x}_{sw} the states related to the switching filter from Section III-C.

The system inputs are defined as

$$\mathbf{u}(k) := [\mathbf{u}_{sw}(k)^\top \quad \mathbf{p}(k)^\top]^\top \in \mathbb{R}^{n_u},$$

where \mathbf{u}_{sw} are the physical switches positions and \mathbf{p} are the three binary inputs entering in the frequency filter from Section III-C. The input dimension is $n_u = 6$. To simplify the notation, let us define the matrices \mathbf{G} and \mathbf{T} to obtain $\mathbf{u}_{sw}(k)$ and $\mathbf{p}(k)$ from $\mathbf{u}(k)$ respectively, i.e.

such that $\mathbf{u}_{sw}(k) = \mathbf{G}\mathbf{u}(k)$ and $\mathbf{p}(k) = \mathbf{T}\mathbf{u}(k)$. Similarly, to obtain $\mathbf{u}_{sw}(k-1)$ from $\mathbf{x}(k)$ we define matrix \mathbf{W} so that $\mathbf{u}_{sw}(k-1) = \mathbf{W}\mathbf{x}(k)$.

The MPC problem with horizon $N \in \mathbb{N}$ can be written as

$$\underset{\mathbf{u}(k)}{\text{minimize}} \quad \sum_{k=0}^{N-1} \gamma^k \ell(\mathbf{x}(k)) + \gamma^N V(\mathbf{x}(N)) \quad (14a)$$

$$\text{subject to} \quad \mathbf{x}(k+1) = \mathbf{A}\mathbf{x}(k) + \mathbf{B}\mathbf{u}(k) \quad (14b)$$

$$\mathbf{x}(0) = \mathbf{x}_0 \quad (14c)$$

$$\mathbf{x}(k) \in \mathcal{X}, \mathbf{u}(k) \in \mathcal{U}(\mathbf{x}_0), \quad (14d)$$

where the stage cost is defined combining the THD and the switching frequency penalties in (9) and (12) respectively

$$\ell(\mathbf{x}(k)) = \|\mathbf{C}\mathbf{x}(k)\|_2^2 = \|\mathbf{e}(k)\|_2^2 + \delta \|e_{sw}(k)\|_2^2.$$

The tail cost $V(\mathbf{x}(N))$ is an approximation of the infinite horizon tail that we will compute in the next section using approximate dynamic programming (ADP). The matrices \mathbf{A} , \mathbf{B} and \mathbf{C} define the extended system dynamics and the output vector; they can be derived directly from the physical model (4) and from the considerations in Sections III-C and III-B.

The input constraint set is denoted as

$$\mathcal{U}(\mathbf{x}_0) = \{ -\mathbf{T}\mathbf{u}(k) \leq \mathbf{u}(k) - \mathbf{W}\mathbf{x}(k) \leq \mathbf{T}\mathbf{u}(k), \quad (15a)$$

$$\|\mathbf{T}\mathbf{u}(k)\|_\infty \leq 1, \quad (15b)$$

$$\mathbf{G}\mathbf{u}(k) \in \{-1, 0, 1\}^3, \quad (15c)$$

where constraint (15a) defines the relationship between \mathbf{u}_{sw} and \mathbf{p} from (10) and (11). Constraint (15b) together with (15a) defines the switching constraints $\|\mathbf{u}_{sw}(k) - \mathbf{u}_{sw}(k-1)\|_\infty \leq 1$ imposed to avoid a shoot through in the inverter positions that could damage the components. Finally, (15c) enforces integrality of the switching positions.

Observe that the controller tuning parameters are δ , which defines the relative importance of the THD and f_{sw} components in the cost function, and r_1, r_2 that shape the switching frequency estimator.

E. Approximate Dynamic Programming

The goal of this section is to compute a value function approximation $V^{adp}(\cdot)$ for an infinite horizon version of (14). The function $V^{adp}(\cdot)$ will be used as a tail cost in (14).

Let $V^*(\mathbf{z})$ be the value function, i.e. the optimal value of the objective of our control problem starting at state $\mathbf{x} = \mathbf{z}$

$$V^*(\mathbf{z}) = \min_{\mathbf{u} \in \mathcal{U}(\mathbf{z})} \left\{ \sum_{k=0}^{\infty} \gamma^k \ell(\mathbf{x}(k), \mathbf{u}(k)) \right\},$$

subject to the system dynamics (14b) and initial state constraint $\mathbf{x}(0) = \mathbf{z}$. For notational convenience, we will drop the time index k from the vectors in this section. The main idea behind dynamic programming is that the function $V^*(\cdot)$ is the unique solution of the equation

$$V^*(\mathbf{z}) = \min_{\mathbf{u} \in \mathcal{U}(\mathbf{z})} \{l(\mathbf{z}, \mathbf{u}) + \gamma V^*(\mathbf{A}\mathbf{z} + \mathbf{B}\mathbf{u})\} \quad \forall \mathbf{z},$$

known as the Bellman equation. The right-hand side can be written as monotonic operator on V^* , usually referred to as the Bellman operator: $V^* = \mathcal{T}V^*$. Once V^* is known, the optimal control policy for our problem starting at state \mathbf{z} can be found as

$$\psi^*(\mathbf{z}) = \arg \min_{\mathbf{u} \in \mathcal{U}(\mathbf{z})} \{l(\mathbf{z}, \mathbf{u}) + \gamma V^*(\mathbf{A}\mathbf{z} + \mathbf{B}\mathbf{u})\},$$

subject to constraints (14b) and $\mathbf{x}(0) = \mathbf{z}$.

Unfortunately, solutions to the Bellman equation can only be solved analytically in a limited number of special cases; e.g. when the state and inputs have small dimensions or when the system is linear, unconstrained and the cost function is quadratic [20]. For more complicated problems, dynamic programming is limited by the so-called curse of dimensionality; storage and computation requirements tend to grow exponentially with the problem dimensions. Because of the integer switches in the power converter analyzed in this work, it is intractable to compute the optimal infinite horizon cost and policy and, hence, systematic methods for approximating the optimal value function offline are needed.

Approximate dynamic programming [12] consists of various techniques for estimating V^* using knowledge from the system dynamics, fitted data through machine learning or iterative learning through simulations.

Approximation via Iterated Bellman Inequalities: the approach developed in [13] and [14] relaxes the Bellman equation into an inequality

$$V^{adp}(\mathbf{z}) \leq \min_{\mathbf{u} \in \mathcal{U}(\mathbf{z})} \{l(\mathbf{z}, \mathbf{u}) + \gamma V^{adp}(\mathbf{A}\mathbf{z} + \mathbf{B}\mathbf{u})\}, \quad \forall \mathbf{z}, \quad (16)$$

or, equivalently, using the Bellman operator: $V^{adp} \leq \mathcal{T}V^{adp}$.

The set of functions V^{adp} that satisfy the Bellman inequality are underestimators of the optimal value function V^* . This happens because, if V^{adp} satisfies $V^{adp} \leq \mathcal{T}V^{adp}$, then by the monotonicity of the operator \mathcal{T} and value iteration convergence, we can write

$$V^{adp} \leq \mathcal{T}V^{adp} \leq \mathcal{T}(\mathcal{T}V^{adp}) \leq \dots \leq \lim_{i \rightarrow \infty} \mathcal{T}^i V^{adp} = V^*.$$

The Bellman inequality is therefore a sufficient condition for underestimation of V^* . In [14] the authors show that by iterating inequality (16), the conservatism of the approximation can be reduced. The iterated bellman inequality is defined as:

$$V^{adp}(\mathbf{z}) \leq \mathcal{T}^M V^{adp}.$$

where $M > 1$ is an integer defining the number of iterations. This inequality is equivalent to the existence of functions V_i^{adp} such that

$$V^{adp} \leq \mathcal{T}V_1^{adp}, \quad V_1^{adp} \leq \mathcal{T}V_2^{adp}, \quad \dots \quad V_{M-1}^{adp} \leq \mathcal{T}V^{adp}.$$

By defining $V_0^{adp} = V_M^{adp} = V^{adp}$, we can rewrite the iterated inequality as

$$V_{i-1}^{adp} \leq \mathcal{T}V_i^{adp}, \quad i = 1, \dots, M, \quad (17)$$

where V_i^{adp} are the iterates of the value function.

To make the problem tractable, we will restrict the iterates to the finite-dimensional subspace spanned by the basis functions $V^{(j)}$ defined in [13], [14]:

$$V_i^{adp} = \sum_{j=1}^K \alpha_{ij} V^{(j)}, \quad i = 0, \dots, M-1. \quad (18)$$

The coefficients α_i will be computed by solving a Semidefinite Program (SDP) [15]. The rewritten iterated Bellman inequality in (17) suggests the following optimization problem for finding the best underestimator for the value function V^*

$$\text{maximize} \quad \int_{\mathcal{X}} V^{adp}(\mathbf{z}) c(d\mathbf{z}) \quad (19a)$$

$$\text{subject to} \quad V_{i-1}^{adp}(\mathbf{z}) \leq \min_{\mathbf{u} \in \mathcal{U}(\mathbf{z})} \left\{ l(\mathbf{z}, \mathbf{u}) + \gamma V_i^{adp}(\mathbf{A}\mathbf{z} + \mathbf{B}\mathbf{u}) \right\} \quad (19b)$$

$$\forall \mathbf{z} \in \mathbb{R}^6 \times \{-1, 0, 1\}, \quad i = 1, \dots, M, \quad (19c)$$

$$V_0^{adp} = V_M^{adp} = V^{adp}, \quad (19d)$$

where $c(\cdot)$ is a non-negative measure over the state space. On the chosen subspace (18), the inequality (19b) is convex in the coefficients α_{ij} . To see this, note that the left-hand side is affine in α_{ij} . Moreover, for a fixed \mathbf{u} the argument of min in the right-hand side is affine in α_{ij} while the min of affine functions is concave.

The solution to (19) is the function spanned by the chosen basis that maximizes the c -weighted 1-norm defined in the cost function while satisfying the iterated Bellman inequality [13]. Hence, $c(\cdot)$ can be thought as a distribution giving more importance to regions of the state space where we would like a better approximation.

Following the approach in [14], we make use of quadratic candidate functions of the form

$$V_i^{adp}(\mathbf{z}) = \mathbf{z}^\top \mathbf{P}_i \mathbf{z} + 2\mathbf{q}_i^\top \mathbf{z} + r_i, \quad i = 0, \dots, M, \quad (20)$$

where $\mathbf{P}_i \in \mathbb{S}^{n_x}$, $\mathbf{q}_i \in \mathbb{R}^{n_x}$, $r_i \in \mathbb{R}$, $i = 0, \dots, M$.

If we denote $\boldsymbol{\mu}_c \in \mathbb{R}^{n_x}$ and $\boldsymbol{\Sigma}_c \in \mathbb{S}_+^{n_x}$ as the mean and the covariance matrix of measure $c(\cdot)$ respectively, by using candidate functions as in (20) the cost function of problem (19) becomes

$$\int_{\mathcal{X}} V^{adp}(\mathbf{z}) c(d\mathbf{z}) = \text{Tr}(\mathbf{P}_0 \boldsymbol{\Sigma}_c) + 2\mathbf{q}_0^\top \boldsymbol{\mu}_c + r_0.$$

We now focus on rewriting the constraint (19b) a Linear Matrix Inequality (LMI) [21]. We first remove the min in the right-hand side by imposing the constraint for every admissible $\mathbf{u} \in \mathcal{U}(\mathbf{x}_0)$ and obtain

$$\begin{aligned} V_{i-1}^{adp}(\mathbf{z}) &\leq l(\mathbf{z}, \mathbf{u}) + \gamma V_i^{adp}(\mathbf{A}\mathbf{z} + \mathbf{B}\mathbf{u}), \\ \forall \mathbf{z} \in \mathbb{R}^6 \times \{-1, 0, 1\}, \forall \mathbf{u} \in \mathcal{U}(\mathbf{z}), & \quad i = 1, \dots, M. \end{aligned} \quad (21)$$

From [14], we can rewrite (21) as a quadratic form

$$\begin{aligned} \begin{bmatrix} \mathbf{z} \\ 1 \end{bmatrix}^\top \mathbf{M}_i(\mathbf{u}) \begin{bmatrix} \mathbf{z} \\ 1 \end{bmatrix} &\geq 0, \quad \forall \mathbf{z} \in \mathbb{R}^6 \times \{-1, 0, 1\}, \\ \forall \mathbf{u} \in \mathcal{U}(\mathbf{z}), \quad i &= 1, \dots, M, \end{aligned} \quad (22)$$

where

$$\mathbf{M}_i(\mathbf{u}) = \mathbf{L} + \gamma \mathbf{G}_i(\mathbf{u}) - \mathbf{S}_{i-1} \in \mathbb{S}^{n_x}. \quad (23)$$

is a symmetric matrix. The matrices \mathbf{S}_{i-1} , \mathbf{L} and $\mathbf{G}_i(\mathbf{u})$ are defined in Appendix B.

By noting that the state vector \mathbf{z} includes two parts which can take only a finite set of values — the normalized desired frequency fixed to 1 and the previous physical input $\mathbf{u}_{sw}(k-1) \in \{-1, 0, 1\}$ — we can explicitly enumerate part of the state-space and rewrite the quadratic form (22) more compactly as

$$\begin{bmatrix} \tilde{\mathbf{z}} \\ 1 \end{bmatrix}^\top \tilde{\mathbf{M}}_i(\mathbf{m}) \begin{bmatrix} \tilde{\mathbf{z}} \\ 1 \end{bmatrix} \geq 0, \quad \forall \tilde{\mathbf{z}} \in \mathbb{R}^8, \quad \forall \mathbf{m} \in \mathcal{M}, \quad i = 1, \dots, M, \quad (24)$$

where $\tilde{\mathbf{z}}$ is the state vector without the desired frequency and $\mathbf{u}_{sw}(k-1)$. Moreover, $\mathbf{m} := (\mathbf{u}_{sw}, \mathbf{u}_{sw,pr}) \in \mathcal{M}$ are all the possible combinations of current and previous physical inputs satisfying the switching and integrality constraints (15). The detailed derivation of $\tilde{\mathbf{M}}(\mathbf{m}) \in \mathbb{S}^9$ can be found in Appendix B.

Using the non-negativity condition of quadratic forms [15], it is easy to see that (24) holds if and only if $\tilde{\mathbf{M}}_i(\mathbf{m})$ is positive semidefinite. Hence, problem (19) can finally be rewritten as the following SDP

$$\begin{aligned} \text{maximize} \quad & \text{Tr}(\mathbf{P}_0 \boldsymbol{\Sigma}_c) + 2\mathbf{q}_0^\top \boldsymbol{\mu}_c + r_0 \\ \text{subject to} \quad & \tilde{\mathbf{M}}_i(\mathbf{m}) \succeq 0, \quad \forall \mathbf{m} \in \mathcal{M}, \quad i = 1, \dots, M \\ & V_0^{adp} = V_M^{adp} \\ & \mathbf{P}_i \in \mathbb{S}^{n_x}, \quad \mathbf{q}_i \in \mathbb{R}^{n_x}, \quad r_i \in \mathbb{R}, \quad i = 0, \dots, M, \end{aligned} \quad (25)$$

which can be solved efficiently using a standard SDP solver, e.g. [22]. Once we obtain the solution to (25), we can define the infinite horizon tail cost to be used in problem (14) as

$$V^{adp}(\mathbf{z}) = \mathbf{z}^\top \mathbf{P}_0 \mathbf{z} + 2\mathbf{q}_0^\top \mathbf{z} + r_0. \quad (26)$$

F. Optimization Problem in Vector Form

Since we consider short horizons, we adopt a condensed MPC formulation of problem (14) with only input variables producing a purely integer program. In this way all the possible discrete input combinations can be evaluated directly. With a sparse formulation including the continuous states within the variables, it would be necessary to solve a mixed-integer program requiring more complex computations.

Let us define the input sequence over the horizon N starting at time 0 as

$$\mathbf{U} = [\mathbf{u}^\top(0) \quad \mathbf{u}^\top(1) \quad \dots \quad \mathbf{u}^\top(N-1)]^\top, \quad (27)$$

where we have dropped the time index from \mathbf{U} to simplify the notation. With straightforward algebraic manipulations outlined in Appendix C, it is possible to rewrite problem (14) as a parametric integer quadratic program in the initial state \mathbf{x}_0

$$\begin{aligned} & \text{minimize} && \frac{1}{2}\mathbf{U}^\top \mathbf{Q}\mathbf{U} + \mathbf{f}(\mathbf{x}_0)^\top \mathbf{U} \\ & \text{subject to} && \mathbf{A}_{ineq}\mathbf{U} \leq \mathbf{b}_{ineq}(\mathbf{x}_0) \\ & && \mathcal{G}\mathbf{U} \in \{-1, 0, 1\}^{3N}. \end{aligned} \tag{28}$$

Following a receding horizon control strategy, at each stage k problem (28) is solved, obtaining the optimal sequence \mathbf{U} from which only the first input $\mathbf{u}(0)$ is applied to the switches. At the next stage $k+1$, given new information on \mathbf{x}_0 , a new optimization problem is then solved providing an updated optimal switching sequence, and so on.

IV. COMPLEXITY ANALYSIS

The structure of problem (28) is highly parallelizable due to the *finite control set* of the solution. Since in this work we consider short control horizons, all the possible control sequences can be evaluated in parallel to determine the optimum. Hence, the computation time required can be drastically reduced.

We now present a brief analysis of the number of floating-point operations (flops) required by a solution approach based on a highly parallelized direct enumeration method. We define a flop as one addition, subtraction or multiplication (no divisions will be required in the algorithm).

We first consider all the operations that can be performed offline. Given all the input combinations $\mathbf{U}_i \in \mathbb{R}^{Nn_u}$, with $i \in \{1, \dots, 27^N\}$, we can precompute for each one part of the cost function $\xi_i = \frac{1}{2}\mathbf{U}_i^\top \mathbf{Q}\mathbf{U}_i$ obtaining a vector $\boldsymbol{\xi} \in \mathbb{R}^{27^N}$. Moreover, all the left hand sides of the inequalities can also be precomputed as $\nu_i = \mathbf{A}_{ineq}\mathbf{U}_i$ resulting in a vector $\boldsymbol{\nu} \in \mathbb{R}^{27^N}$.

Before the evaluation of the possible input sequences, at each time step we must compute $\mathbf{f}(\mathbf{x}_0)$ and $\mathbf{b}_{ineq}(\mathbf{x}_0)$ depending on the initial state \mathbf{x}_0 . From (36) we can write $\mathbf{f}(\mathbf{x}_0)$ as $\mathbf{f}(\mathbf{x}_0) = \boldsymbol{\Theta}\mathbf{x}_0 + \boldsymbol{\zeta}$, which is a matrix-vector multiplication and an addition requiring $Nn_u(2n_x - 1)$ and n_u flops respectively. The part of $\mathbf{b}_{ineq}(\mathbf{x}_0)$ depending on \mathbf{x}_0 is, as in (37), $\mathcal{S}\mathbf{A}\mathbf{x}_0$. This is a matrix-vector multiplication requiring $2Nn_u(2n_x - 1)$ flops. The number of flops required to construct $\mathbf{f}(\mathbf{x}_0)$ and $\mathbf{b}_{ineq}(\mathbf{x}_0)$ is $N_{\mathbf{x}_0} = 3Nn_u(2n_x - 1) + n_u$.

We can now consider the evaluation of each control sequence \mathbf{U}_i that can be performed in parallel. If the \mathbf{U}_i satisfies the constraint $\mathbf{A}_{ineq}\mathbf{U}_i \leq \mathbf{b}_{ineq}(\mathbf{x}_0)$, then we can proceed in computing the cost function value $J_i = z_i + \mathbf{f}(\mathbf{x}_0)^\top \mathbf{U}_i$ which corresponds to a vector multiplication and a scalar addition of $N_J = 2(Nn_u - 1) + 1$ flops in total. If the current value of J_i is higher than the current cost function minimum, it will be saved as the best solution candidate.

By assuming enough resources to parallelize each J_i computation, which is the case for short horizons, then the total number of serial flops to obtain the optimal switching sequence is:

$$N_{tot} = N_{x_0} + N_J = Nn_u(6n_x - 1) + n_u - 1. \quad (29)$$

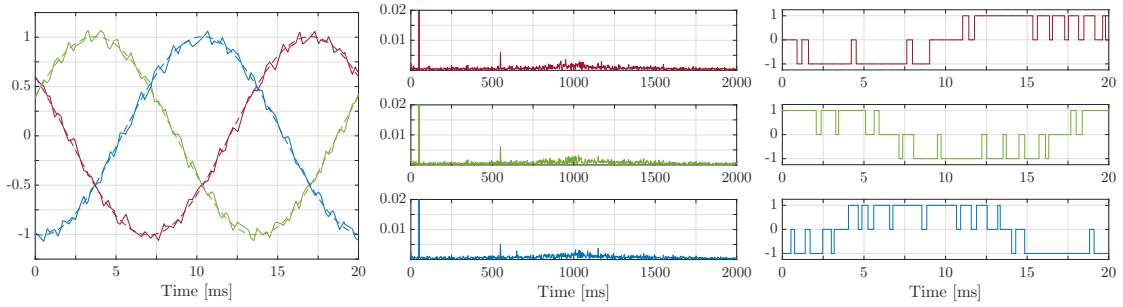
Since $n_x = 12$ and $n_u = 6$, $N_{tot} = 426N + 5$. In order to obtain a very rough estimate of the running time required by the algorithm, let us consider a typical modern FPGA platform [23] running at 400 MHz (2.5 ns per clock cycle) where a floating-point operation would require in general 14 cycles [24]. With our approach it is possible to use very short horizons in order to get good control performances. Hence, by choosing horizon $N = 1$, if we consider roughly a clock cycle per serial flop operation, the estimated number of clock cycles needed to perform N_{tot} flops is $N_{cyc} = 6034$, which corresponds to a time of $T_{op} = 15.08 \mu\text{s}$. Thus, the controller is able to solve the optimization problem within the required sampling time T_s .

The number of flops in (29) leads to a very conservative estimate of the time required and can be drastically reduced. First, by considering adder reduction trees, the additions in the matrix-vector and vector multiplications can be performed in a parallel fashion requiring $\lceil \log_2(n_v) \rceil$ parallel flops where n_v is the dimension of the vectors involved. Second, since the optimization variables \mathbf{U}_i are composed only of -1 , 0 or 1 scalars, the multiplications could be significantly simplified by exploiting the binary representations of the variables on an embedded platform. Last, fixed-point operations requiring only a single clock cycle could be adopted instead of flops, leading to large potential reductions in computation time.

We now compare the complexity of the sphere decoding algorithm presented in [8] by following the analysis in [25]. Note that the sphere decoding algorithm is serial and does not offer the same parallelization options as the approach proposed in this work. Thus, it is not possible to implement it on a FPGA board exploiting the hardware architecture [24] to speedup the execution time to the same degree. Given $\mu \in \mathbb{N}$ as the number of visited nodes in the branch-and-bound algorithm, we can give an estimate of the floating point operations required to obtain the optimal switching sequence. By construction, at each level of the branch-and-bound algorithm, the dimension of the control vector \mathbf{U}_i is augmented scalar by scalar from 1 to $3N$. We will denote the dimension of \mathbf{U}_i at level j as m_j . We can write the total number flops according to [25] as:

$$N_{sphdec} = 9(N^2 + \mu) + 3 \left(-1 + \sum_{\substack{\text{explored nodes with} \\ j=2, \dots, 3N}} m_j \right).$$

By considering the most favorable case in which the first branch-and-bound feasible solution is the optimal one, the number of explored nodes is $\mu = 3N$ and we need to compute the



(a) Three-phase stator currents (solid lines) with their references (dashed lines).

(b) Stator current spectrum.

(c) Three-phase switching position inputs.

Fig. 3. Simulated waveforms produced by the direct model predictive controller at steady state operation, at full speed and rated torque. Horizon of $N = 1$ is used. The switching frequency is approximately 300 Hz and the current THD is 5.24 %.

following number of flops:

$$\begin{aligned}
 N_{sphdec} &= 9(N^2 + 3N) + 3 \left(-1 + \sum_{j=2}^{3N-1} j \right) \\
 &= 9(N^2 + 3N) + 3 \frac{(3N-1)3N}{2} - 6 \\
 &= \frac{45}{2}(N^2 + N) - 6
 \end{aligned}$$

In general, with the formulation in [8], it is necessary to choose long prediction horizons to obtain good control performance. A horizon of $N = 7$ would correspond to a $N_{sphdec} = 1254$ number of flops, in the most favorable case of directly finding the optimal solution. With the same considerations as before, this would translate to a computation time of $T_{op} = 43.9 \mu\text{s}$, which is more than the sampling time required. Recall that it is very unlikely that the optimal solution in a branch-and-bound algorithm will correspond to the first feasible solution found and that the number of nodes visited can be much higher — up to 27^N in the worst case.

V. FRAMEWORK FOR PERFORMANCE EVALUATION

We run simulations on a model of a neutral point clamped voltage source inverter connected with a medium-voltage induction machine and a constant mechanical load. As a typical medium-voltage induction machine example, we use the same model as in [8]: a 3.3 kW and 50 Hz squirrel-cage induction machine rated at 2 MVA with total leakage inductance of 0.25 pu. On the inverter side, we assume the dc-link voltage $V_{dc} = 5.2 \text{ kV}$ to be constant and the potential of the neutral point N to be fixed. The base quantities of the per unit (pu) system are the following: $V_B = \sqrt{2/3}V_{rat} = 2694 \text{ V}$, $I_B = \sqrt{2}I_{rat} = 503.5 \text{ A}$ and $f_B = f_{rat} = 50 \text{ Hz}$. Quantities V_{rat} , I_{rat} and f_{rat} refer to the rated voltage, current and frequency respectively. The detailed parameters are in Table I. Frequency ranges between 200

and 350 Hz are of particular importance for medium-voltage inverters [8]. For the current model, the state of the art approaches reach THDs between 7 and 4%.

TABLE I
RATED VALUES AND PARAMETERS OF THE DRIVE [8]

Induction Motor		Inverter			
Voltage	3300 V	r_s	0.0108 pu	V_{dc}	1.930 pu
Current	356 A	r_r	0.0091 pu	x_c	11.769 pu
Real power	1.587 MW	x_{ls}	0.1493 pu		
Apparent power	2.035 MVA	x_{lr}	0.1104 pu		
Frequency	50 Hz	x_m	2.3489 pu		
Rotational speed	596 rpm				

The simulations are run in MATLAB, using an idealized model with the semiconductors switching instantaneously. This is motivated by the fact that, using a similar model, previous simulations [26] showed a very closed match with the experimental results in [27]. As such, we neglect second-order effects like deadtimes, controller delays, measurement noise, observer errors, saturation of the machine's magnetic material, variations of the parameters and so on, without losing the significance of the results. In addition, if not otherwise stated, all simulations were done at rated torque, nominal speed, fundamental frequency of 50 Hz and rated currents. The infinite horizon estimation SDP (25) is formulated in MATLAB using YALMIP [28] and solved offline using MOSEK [22].

VI. SIMULATION RESULTS

A. Steady State Performance

The steady-state performance of the system with the proposed method is shown in Figure 3. The discount factor is chosen as $\gamma = 0.95$, the switching frequency filter parameters as $r_1 = r_2 = 800$ in order to get a smooth estimate. The desired switching frequency is set to 300 Hz and the weighting δ is chosen such that the obtained frequency lies within 300 ± 10 Hz. The simulation results for $N = 1$ are shown in Figure 3 in the (pu) system. The three-phase stator currents are displayed over a fundamental period in Figure 3a, the three spectra are shown in Figure 3b with THD of 5.24% and the input sequences are plotted in Figure 3c.

For comparison, we simulate the drive system also with the controller discussed in [8] denoted as SphDec tuned in order to have the same switching frequency by adjusting the weighting parameter λ_u .

Numerical results with both approaches are presented in Table II. Our method, with a horizon of $N = 1$ provides at the same time a THD improvement over the direct MPC formulation in [8] with $N = 10$ and a drastically better numerical speed. This shows how choosing a meaningful cost function can provide good control performances without resorting to long horizons. Moreover, we also perform a comparison with longer horizons $N = 2$, $N = 3$

TABLE II
SIMULATION RESULTS WITH APPROXIMATE DYNAMIC PROGRAMMING APPROACH AND WITH SPHDEC
FROM [9]

	ADP		SphDec [9]	
	δ	THD [%]	λ_u	THD [%]
$N = 1$	4	5.24	0.0023	5.44
$N = 2$	5.8	5.18	0.0069	5.43
$N = 3$	8	5.05	0.0136	5.42
$N = 10$	35	5.02	0.1025	5.39

and $N = 10$. The results show that, if our method were applied on the drive system with horizon $N = 3$, it would show a clear improvement over the SphDec technique leading to a THD of 5.05%. Horizon $N = 10$ would give an even greater reduction in THD until 5.02%. Furthermore, it is important to underline that the method we propose is the *only* method available that can produce integer optimal solutions to this problem in $25 \mu\text{s}$ sampling time.

B. Performance During Transients

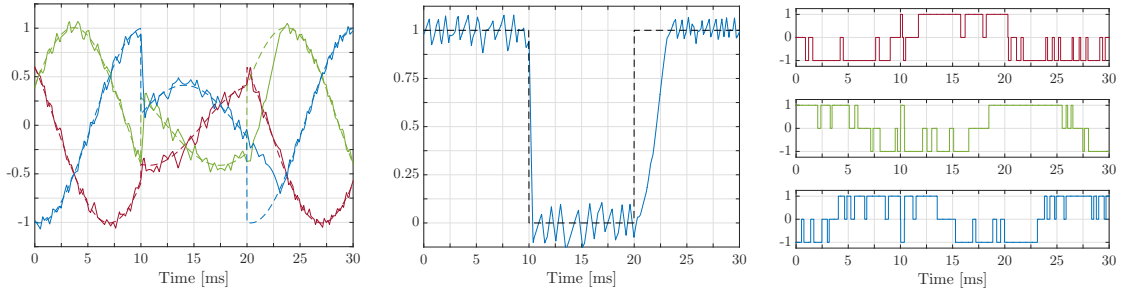
One of the main advantages of direct MPC is the fast transient response [8]. We simulated the system with the same tuning parameters as in the steady state benchmarks. At nominal speed, reference torque steps are imposed, see Figure 4b. These steps are translated into different current references to track, as shown in Figure 4a, while the computed inputs are shown in 4c.

The torque step from 1 to 0 presents an extremely short settling time of 0.35 ms similar to deadbeat control approaches [29]. This is achieved by inverting the voltage applied to the load. Since we prohibited switchings between -1 and 1 in (15a) and (15b), the voltage inversion is performed in $2T_s$ via an intermediate zero switching position.

Switching from 0 to 1 torque produces much slower response time of approximately 3.5 ms. This is due to the limited available voltage in the three-phase admissible switching positions. As shown in Figure 4c, during the second switching at time 20 ms, the last two phases inputs saturate to values $+1$ and -1 respectively for the majority of the transient providing the maximum available voltage that could steer the currents to the desired direction.

We simulated the transient responses also for horizon $N = 10$ obtaining nearly identical settling times. This is because the benefit of longer prediction obtainable by extending the horizon or adopting a powerful final stage costs is reduced by the saturation of the inputs during the transients.

From what we expected from the saturating inputs behavior, these transient results match the simulations of SphDec method from [8] in terms of settling time. This shows that our method does not slow down the fast dynamical behavior during transients typical of direct current MPC.



(a) Three-phase stator currents (solid lines) with their references (dashed lines).

(b) Simulated (solid line) and reference (dashed line) torque.

(c) Three-phase switching position inputs.

Fig. 4. Reference torque steps produced by the direct model predictive controller with horizon $N = 1$.

Finally, the proposed approach showed far superior performance than offline methods for open-loop switch sequence computations like Optimized Pulse Patterns (OPPs). Although these techniques are particularly suited for steady state operation, they perform poorly in terms of robustness and torque transients settling time. To overcome this problem, OPPs has been combined in the past with a modulator driven by a very slow control loop [30]. Some recent contributions on OPPs [31]–[33] have managed to reduce the settling times, although without matching the performance of direct current MPC.

VII. CONCLUSION AND FUTURE WORK

This work proposes a new computationally efficient direct model predictive control (MPC) scheme for current reference tracking in power converters. We extended problem formulation in [8] and [9] in order to include a switching frequency estimator in the system state and rewrite the optimal control problem as a regulation one. To reduce the horizon length and decrease the computational burden while preserving good control performances, we estimated the infinite horizon tail cost of the MPC problem formulation using approximate dynamic programming (ADP).

Steady state simulation results show that with our method requiring short horizons and extremely inexpensive computations, it is possible to obtain better performance than the direct MPC formulation in [8] with long horizons. This is due to the predictive behavior of the tail cost function obtained with ADP. We also performed transient simulations where the proposed approach does not reduce the very fast dynamic response of the direct MPC in [8]. Moreover, from our complexity analysis we show that, in contrast to the previously proposed methods, this algorithm can be easily implemented on embedded platforms like FPGAs and run comfortably within $25 \mu\text{s}$ sampling time.

There are several future work directions to be investigated. First, given the system design there are several symmetries in the model that could be exploited to increase the controller horizon without requiring more computational power. Regarding the frequency estimation,

other filters with different orders could be implemented and their parameters chosen optimally by solving an optimization problem instead of performing manual tuning. Moreover, it would be interesting to benchmark other ADP tail cost functions (e.g. higher order polynomials) to understand which ones best approximate the infinite horizon tail cost and produce the best overall control performance.

APPENDIX A PHYSICAL SYSTEM MATRICES

The matrices corresponding to the continuous-time physical system in (3) are

$$\mathbf{D} = \begin{bmatrix} -\frac{1}{\tau_s} & 0 & \frac{X_m}{\tau_r D} & \omega_r \frac{X_m}{D} \\ 0 & -\frac{1}{\tau_s} & -\omega_r \frac{X_m}{D} & \frac{X_m}{\tau_r D} \\ \frac{X_m}{\tau_r} & 0 & -\frac{1}{\tau_r} & -\omega_r \\ 0 & \frac{X_m}{\tau_r} & \omega_r & -\frac{1}{\tau_r} \end{bmatrix}$$

$$\mathbf{E} = \frac{X_r V_{dc}}{D} \frac{1}{2} \begin{bmatrix} 1 & 0 \\ 0 & 1 \\ 0 & 0 \\ 0 & 0 \end{bmatrix} \mathbf{P}, \quad \mathbf{F} = \begin{bmatrix} 1 & 0 & 0 & 0 \\ 0 & 1 & 0 & 0 \end{bmatrix}.$$

APPENDIX B ADP FORMULATION

The matrix defining the quadratic form are

$$\mathbf{S}_{i-1} := \begin{bmatrix} \mathbf{P}_{i-1} & \mathbf{q}_{i-1} \\ \mathbf{q}_{i-1}^\top & r_{i-1} \end{bmatrix}, \quad \mathbf{L} := \begin{bmatrix} \mathbf{C}^\top \mathbf{C} & \mathbf{0}_{n_x \times 1} \\ \mathbf{0}_{n_x \times 1}^\top & 0 \end{bmatrix}$$

$$\mathbf{G}_i(\mathbf{u}) := \begin{bmatrix} \Psi^{(i)} & \Phi^{(i)}(\mathbf{u}) \\ \Phi^{(i)}(\mathbf{u})^\top & \Gamma^{(i)}(\mathbf{u}) \end{bmatrix},$$

with

$$\Psi^{(i)} = \mathbf{A}^\top \mathbf{P}_{i-1} \mathbf{A}$$

$$\Phi^{(i)}(\mathbf{u}) = \mathbf{A}^\top \mathbf{P}_i \mathbf{B} \mathbf{u} + \mathbf{A}^\top \mathbf{q}_i$$

$$\Gamma^{(i)}(\mathbf{u}) = \mathbf{u}^\top \mathbf{B}^\top \mathbf{P}_i \mathbf{B} \mathbf{u} + 2\mathbf{q}_i^\top \mathbf{B} \mathbf{u} + r_i,$$

for $i = 1, \dots, M$.

The quadratic form decomposition can be derived as follows. For every $\mathbf{m} = (\mathbf{u}_{sw}, \mathbf{u}_{sw,pr}) \in \mathcal{M}$, we can define the input

$$\mathbf{u}_m = \begin{bmatrix} \mathbf{u}_{sw} \\ \|\mathbf{u}_{sw} - \mathbf{u}_{sw,pr}\|_1 \end{bmatrix},$$

and the matrix $M_i(\mathbf{u}_m)$ using (23). Now we can decompose the vector in quadratic form (22) using the state definition (13)

$$[\mathbf{z}^\top \ 1]^\top = [\mathbf{z}_{ph}^\top \ \mathbf{z}_{osc}^\top \ \mathbf{z}_{sw,1:2}^\top \ \mathbf{z}_{sw,3}^\top \ \mathbf{z}_{upr}^\top \ 1]^\top.$$

The matrix $M_i(\mathbf{u}_m)$ can also be decomposed in the same fashion into smaller block matrices as follows

$$\begin{bmatrix} \mathbf{z}_{ph} \\ \mathbf{z}_{osc} \\ \mathbf{z}_{sw,1:2} \\ \mathbf{z}_{sw,3} \\ \mathbf{z}_{upr} \\ 1 \end{bmatrix}^\top \begin{bmatrix} M_{i,11} & M_{i,12} & M_{i,13} & M_{i,14} \\ \hline M_{i,12}^\top & M_{i,22} & M_{i,23} & M_{i,24} \\ M_{i,13}^\top & M_{i,23}^\top & M_{i,33} & M_{i,34} \\ M_{i,14}^\top & M_{i,24}^\top & M_{i,34}^\top & M_{i,44} \end{bmatrix} \begin{bmatrix} \mathbf{z}_{ph} \\ \mathbf{z}_{osc} \\ \mathbf{z}_{sw,1:2} \\ \mathbf{z}_{sw,3} \\ \mathbf{z}_{upr} \\ 1 \end{bmatrix} \geq 0,$$

where the dependency $M_{i,**}(\mathbf{u}_m)$, $\mathbf{m} \in \mathcal{M}$ has been neglected to simplify the notation. The first row and first column block matrices have the first and second dimensions respectively equal to the length of vector $[\mathbf{z}_{ph}^\top \ \mathbf{z}_{osc}^\top \ \mathbf{z}_{sw,1:2}^\top]^\top$. Since $\mathbf{z}_{upr} = \mathbf{u}_{sw,pr}$ and $\mathbf{z}_{sw,3} = 1$ (normalized desired switching frequency), we can rewrite the quadratic form as

$$\begin{bmatrix} \mathbf{z}_{ph} \\ \mathbf{z}_{osc} \\ \mathbf{z}_{sw,1:2} \\ 1 \end{bmatrix}^\top \begin{bmatrix} M_{i,11} & \Psi_{i,1} \\ \hline \Psi_{i,1}^\top & \Psi_{i,2} \end{bmatrix} \begin{bmatrix} \mathbf{z}_{ph} \\ \mathbf{z}_{osc} \\ \mathbf{z}_{sw,1:2} \\ 1 \end{bmatrix} \geq 0, \quad (30)$$

where

$$\Psi_{i,1} = M_{i,13}\mathbf{z}_{upr} + M_{i,12} + M_{i,14}$$

$$\begin{aligned} \Psi_{i,2} &= \mathbf{z}_{upr}^\top M_{i,33} \mathbf{z}_{upr} + 2M_{i,23} \mathbf{z}_{upr} + 2M_{i,34}^\top \mathbf{z}_{upr} \\ &\quad + 2M_{i,24} + M_{i,22} \end{aligned}$$

Therefore, we will denote the matrix in (30) as $\tilde{M}_i(\mathbf{m})$ and the quadratic form vectors as $[\tilde{\mathbf{z}}^\top \ 1]^\top$.

APPENDIX C DENSE FORMULATION OF THE MPC PROBLEM

By considering the input sequence (27) and the state sequence over the horizon denoted as

$$\mathbf{X} = [\mathbf{x}^\top(0) \ \mathbf{x}^\top(1) \ \dots \ \mathbf{x}^\top(N)]^\top,$$

the system dynamics (14b) with initial state constraint (14c) can be written as

$$\mathbf{X} = \mathcal{A}\mathbf{x}_0 + \mathcal{B}\mathbf{U}, \quad (31)$$

where \mathcal{A} and \mathcal{B} are

$$\mathcal{A} := \begin{bmatrix} \mathbf{I} \\ \mathbf{A} \\ \vdots \\ \mathbf{A}^N \end{bmatrix}, \quad \mathcal{B} := \begin{bmatrix} \mathbf{0} & \dots & \mathbf{0} \\ \mathbf{B} & & \vdots \\ \mathbf{AB} & \mathbf{B} & \\ \vdots & \ddots & \ddots & \mathbf{0} \\ \mathbf{A}^{N-1}\mathbf{B} & \dots & \mathbf{AB} & \mathbf{B} \end{bmatrix}.$$

Let us separate cost function (14a) in two parts: the cost from stage 0 to $N - 1$ and the tail cost. The former can be rewritten as

$$\begin{aligned} \sum_{k=0}^{N-1} \gamma^k \|\mathbf{C}\mathbf{x}(k)\|_2^2 &= \mathbf{X}^\top \mathcal{H} \mathbf{X} \\ &= \mathbf{U}^\top \mathcal{B}^\top \mathcal{H} \mathcal{B} \mathbf{U} + 2 \left(\mathcal{B}^\top \mathcal{H} \mathcal{A} \mathbf{x}_0 \right)^\top \mathbf{U} + \text{const}(\mathbf{x}_0), \end{aligned} \quad (32)$$

where last equality is obtained by plugging in (31) and the term $\text{const}(\mathbf{x}_0)$ is a constant depending on the initial state. Matrix \mathcal{H} is defined as

$$\mathcal{H} = \begin{bmatrix} \mathbf{C}^\top \mathbf{C} & & & & \mathbf{0} \\ & \gamma \mathbf{C}^\top \mathbf{C} & & & \vdots \\ & & \ddots & & \\ & & & \gamma^{N-1} \mathbf{C}^\top \mathbf{C} & \\ \mathbf{0} & & \dots & & \mathbf{0} \end{bmatrix}. \quad (33)$$

In order derive the tail cost, let us write last stage as

$$\mathbf{x}(N) = \mathbf{A}^N \mathbf{x}_0 + \mathcal{B}_{end} \mathbf{U}, \quad (34)$$

where \mathcal{B}_{end} is the last row of \mathcal{B} used to compute last state. Using equations (34) and (26), the tail cost can be rewritten as

$$\begin{aligned} V^{adp}(\mathbf{x}(N)) &= \mathbf{x}(N)^\top \mathbf{P}_0 \mathbf{x}(N) + 2 \mathbf{q}_0^\top \mathbf{x}(N) + r_0 \\ &= \mathbf{U}^\top \left(\mathcal{B}_{end}^\top \mathbf{P}_0 \mathcal{B}_{end} \right) \mathbf{U} + 2 \left(\mathcal{B}_{end}^\top \mathbf{P}_0 \mathbf{A}^N \mathbf{x}_0 + \mathcal{B}_{end}^\top \mathbf{q}_0 \right)^\top \mathbf{U} \\ &\quad + \text{const}(\mathbf{x}_0). \end{aligned} \quad (35)$$

By combining (32) and (35) according to (14a), we obtain the full cost function

$$\mathbf{J} = \mathbf{U}^\top \mathbf{Q} \mathbf{U} + 2 \mathbf{f}(\mathbf{x}_0)^\top \mathbf{U} + \text{const}(\mathbf{x}_0),$$

with

$$\begin{aligned} \mathbf{Q} &= \mathcal{B}^\top \mathcal{H} \mathcal{B} + \gamma^N \mathcal{B}_{end}^\top \mathbf{P}_0 \mathcal{B}_{end} \\ \mathbf{f}(\mathbf{x}_0) &= \left(\mathcal{B}^\top \mathcal{H} \mathcal{A} + \gamma^N \mathcal{B}_{end}^\top \mathbf{P}_0 \mathbf{A}^N \right) \mathbf{x}_0 \\ &\quad + \gamma^N \mathcal{B}_{end}^\top \mathbf{q}_0. \end{aligned} \quad (36)$$

We now rewrite the constraints of problem (14) in vector form. Inequalities (15a) with $k = 0, \dots, N - 1$ can be written as

$$\mathcal{R} \mathbf{U} \leq \mathcal{S} \mathbf{X} \iff (\mathcal{R} - \mathcal{S} \mathcal{B}) \mathbf{U} \leq \mathcal{S} \mathcal{A} \mathbf{x}_0, \quad (37)$$

where in the term on the right we substituted (31).

Similarly, constraint (15b) with $k = 0, \dots, N - 1$ can be written

$$\|\mathcal{T} \mathbf{u}(k)\|_\infty \leq 1 \iff \mathcal{T} \mathbf{U} \leq \mathbf{1}, \quad (38)$$

- [6] M. Morari and J. H. Lee, "Model predictive control: past, present and future," *Computers & Chemical Engineering*, vol. 23, no. 4-5, pp. 667–682, 1999.
- [7] P. Karamanakos, T. Geyer, N. Oikonomou, F. D. Kieferndorf, and S. Manias, "Direct Model Predictive Control: A Review of Strategies That Achieve Long Prediction Intervals for Power Electronics," *IEEE Industrial Electronics Magazine*, vol. 8, no. 1, pp. 32–43, Mar. 2014.
- [8] T. Geyer and D. E. Quevedo, "Multistep Finite Control Set Model Predictive Control for Power Electronics," *IEEE Transactions on Power Electronics*, vol. 29, no. 12, pp. 6836–6846.
- [9] —, "Performance of Multistep Finite Control Set Model Predictive Control for Power Electronics," *IEEE Transactions on Power Electronics*, vol. 30, no. 3, pp. 1633–1644.
- [10] B. Hassibi and H. Vikalo, "On the sphere-decoding algorithm I. Expected complexity," *IEEE Transactions on Signal Processing*, vol. 53, no. 8, pp. 2806–2818, Jul. 2005.
- [11] S. Kouro, P. Cortes, R. Vargas, U. Ammann, and J. Rodriguez, "Model Predictive Control - A Simple and Powerful Method to Control Power Converters," *IEEE Transactions on Industrial Electronics*, vol. 56, no. 6, pp. 1826–1838, May 2009.
- [12] D. P. Bertsekas, *Dynamic programming and optimal control*. Athena Scientific Belmont, Massachusetts, 1996.
- [13] D. P. de Farias and B. Van Roy, "The linear programming approach to approximate dynamic programming," *Operations Research*, 2003.
- [14] Y. Wang, B. O'Donoghue, and S. Boyd, "Approximate dynamic programming via iterated Bellman inequalities," *International Journal of Robust and Nonlinear Control*, 2014.
- [15] L. Vandenberghe and S. Boyd, "Semidefinite Programming," *SIAM Review*, vol. 38, no. 1, pp. 49–95, 1996.
- [16] P. C. Krause, O. Wasynczuk, and S. D. Sudhoff, *Analysis of Electric Machinery and Drive Systems*, 2nd ed. Hoboken, NJ, USA: Wiley, 2002.
- [17] J. Holtz, "The representation of AC machine dynamics by complex signal flow graphs," *IEEE Transactions on Industrial Electronics*, vol. 42, no. 3, pp. 263–271, 1995.
- [18] W. C. Duesterhoeft, M. W. Schulz, and E. Clarke, "Determination of Instantaneous Currents and Voltages by Means of Alpha, Beta, and Zero Components," *American Institute of Electrical Engineers, Transactions of the*, vol. 70, no. 2, pp. 1248–1255, Jul. 1951.
- [19] A. V. Oppenheim and A. S. Willsky, *Signals and Systems*, 2nd ed. Upper Saddle River, NJ, USA: Prentice-Hall, Inc., 1997.
- [20] R. E. Kalman, "When Is a Linear Control System Optimal?" *Journal of Basic Engineering*, vol. 86, no. 1, pp. 51–60, 1964.
- [21] S. Boyd, L. El Ghaoui, E. Feron, and V. Balakrishnan, "Linear Matrix Inequalities in System and Control Theory," 1994.
- [22] MOSEK ApS, *The MOSEK optimization toolbox for MATLAB manual. Version 7.1 (Revision 35)*., 2015.
- [23] Xilinx, Inc., *LogiCORE IP Floating-Point Operator v7.0*, Mar. 2014.
- [24] J. L. Jerez, P. J. Goulart, S. Richter, G. A. Constantinides, E. C. Kerrigan, and M. Morari, "Embedded Online Optimization for Model Predictive Control at Megahertz Rates," *IEEE Transactions on Automatic Control*, vol. 59, no. 12, pp. 3238–3251, Nov. 2014.
- [25] P. Karamanakos, T. Geyer, and R. Kennel, "Reformulation of the long-horizon direct model predictive control problem to reduce the computational effort," in *Energy Conversion Congress and Exposition (ECCE)*. IEEE, 2014, pp. 3512–3519.

- [26] T. Geyer, G. Papafotiou, and M. Morari, "Model Predictive Direct Torque Control - Part I: Concept, Algorithm, and Analysis," *IEEE Transactions on Industrial Electronics*, vol. 56, no. 6, pp. 1894–1905, May 2009.
- [27] G. Papafotiou, J. Kley, K. G. Papadopoulos, P. Bohren, and M. Morari, "Model Predictive Direct Torque Control - Part II: Implementation and Experimental Evaluation," *IEEE Transactions on Industrial Electronics*, vol. 56, no. 6, pp. 1906–1915, May 2009.
- [28] J. Löfberg, "YALMIP : A Toolbox for Modeling and Optimization in MATLAB," in *Proceedings of the CACSD Conference*, Taipei, Taiwan, 2004.
- [29] J. Rodriguez and P. Cortes, *Predictive control of power converters and electrical drives*. John Wiley & Sons, 2012, vol. 40.
- [30] J. Holtz and B. Beyer, "Fast current trajectory tracking control based on synchronous optimal pulsewidth modulation," *IEEE Transactions on Industry Applications*, vol. 31, no. 5, pp. 1110–1120, 1995.
- [31] J. Holtz and N. Oikonomou, "Synchronous Optimal Pulsewidth Modulation and Stator Flux Trajectory Control for Medium-Voltage Drives," *IEEE Transactions on Industry Applications*, vol. 43, no. 2, pp. 600–608, Mar. 2007.
- [32] T. Geyer, N. Oikonomou, G. Papafotiou, and F. D. Kieferndorf, "Model Predictive Pulse Pattern Control," *IEEE Transactions on Industry Applications*, vol. 48, no. 2, pp. 663–676, Mar. 2012.
- [33] N. Oikonomou, C. Gutscher, P. Karamanakos, F. D. Kieferndorf, and T. Geyer, "Model Predictive Pulse Pattern Control for the Five-Level Active Neutral-Point-Clamped Inverter," *IEEE Transactions on Industry Applications*, vol. 49, no. 6, pp. 2583–2592, Oct. 2013.